nature portfolio

https://doi.org/10.1038/s41567-022-01628-6

Supplementary information

Origin of the boson peak in amorphous solids

In the format provided by the authors and unedited

Supplementary Information for "Origin of the Boson peak in amorphous solids"

Yuan-Chao Hu[1] and Hajime Tanaka[1,2,*]

[1] *Department of Fundamental Engineering, Institute of Industrial Science, University of Tokyo, 4-6-1 Komaba, Meguro-ku, Tokyo 153-8505, Japan*

[2] *Research Center for Advanced Science and Technology, University of Tokyo, 4-6-1 Komaba, Meguro-ku, Tokyo 153-8904, Japan*

(Dated: September 8, 2021)

Contents

* E-mail: tanaka@iis.u-tokyo.ac.jp

I. Characterisation of the dynamics and structure

To obtain the glass transition temperature T_g of the 2DPL model and better discuss the glassy states, we characterise the dynamical properties in the supercooled liquid states. Following the standard methods, we calculate the self-intermediate scattering functions with cage-relative motions to eliminate the Mermin-Wagner fluctuations in two dimensions:

$$F_s(q,t) = \frac{1}{N}\left\langle \sum_{j=1}^{N} \exp\left[i\vec{q}\cdot\Delta\vec{r}_j(t)\right]\right\rangle, \tag{S1}$$

and the mean-square displacement by

$$\langle \Delta r^2(t)\rangle = \frac{1}{N}\left\langle \sum_{j=1}^{N} \left[\vec{r}_j(t)-\vec{r}_j(0)\right]^2\right\rangle. \tag{S2}$$

Here $\vec{q}$ is the wavevector corresponding to the first peak of the static structure factor (see Supplementary Fig. S1). $F_s(q,t)$ at various temperatures are shown in Supplementary Fig. S2a. We define the structural relaxation time τ_α as $F_s(q,\tau_\alpha) = 1/e$. The obtained τ_α can be generally described by the Vogel-FulcherTammann (VFT) equation (see Extended Data Fig. 1a):

$$\tau_\alpha = \tau_0 \exp\left(\frac{DT_0}{T-T_0}\right), \tag{S3}$$

in which D is the fragility index and T_0 (=0.31) is the hypothetical ideal glass-transition temperature. In this way, we define $T_g = 0.44$ from $\tau_\alpha(T_g) = 10^6$, which is close to the previous studies [1, 2]. We note that at $T = 1.0$, $\tau_\alpha = 5.0$. We also show the temperature-dependent mean-square displacements in Supplementary Fig. S2b to quantify the Debye-Waller factor μ^{DW} of the entire material at a caging time. A universally quantitative correlation between τ_α and μ^{DW} has been found as (see Extended Data Fig. 1b)

$$\tau_\alpha = \tau_A \exp[(\mu_A^2/\mu^{\mathrm{DW}})^{\alpha/2} - 1], \tag{S4}$$

which holds in many systems, such as metallic glasses and a crystalline material (superionic UO_2) [3–6].

To characterize the glassy nature of our low temperature solids at $T = 0.1$, we first show the exponential decay of the pair correlation function $g(r)-1$ in Supplementary Fig. S2c. It

unambiguously indicates the absence of translational order in our system. We also calculate the local hexatic order parameter by

$$\psi_6^j = \frac{1}{N_j} \sum_{m=1}^{N_j} e^{i6\theta_m^j}, \tag{S5}$$

in which N_j is the number of nearest neighbours of particle j, and θ_m^j is the angle between the positional vector $\vec{r}_{jm}$ and the horizontal axis. We show the spatial distribution of the local hexatic order $|\psi_6|$ in Supplementary Fig. S2d. We can see that the hexatic order is barely developed in the glassy state of our binary mixture. To make this quantitative, we characterise its spatial correlation by

$$\frac{g_6(r)}{g(r)} = \frac{\sum_{j\neq k} \delta(r - |\vec{r}_{jk}|)\psi_6^j \psi_6^{k*}}{\sum_{j\neq k} \delta(r - |\vec{r}_{jk}|)}, \tag{S6}$$

which is shown in Supplementary Fig. S2e with the fitting to e^{-r/ξ_6}. The spatial correlation length of the hexatic order ξ_6 is very short, comparable to one or two particle sizes. These results are consistent with those of the "2dR10" model in Ref. [7]. Thus, we may conclude that our system size is large enough to have the complete statistics of the disorder.

We also show the transverse and longitudinal dynamic structure factors in the low q region in Supplementary Fig. S3. The properties of the normal modes of two atomic species of this system are also shown in Supplementary Fig. S4.

II. Finite-size effect

To consider the finite-size effect on our findings in the main text, we carry out additional simulations with a total of $N = 32768$ atoms, with 10 independent runs, in the same procedure. Because of the large system size, we only extract the vibrational modes at low frequencies by diagonalising the Hessian matrix of the inherent structure. We first show the vibrational density of state (VDOS) in Supplementary Fig. S5a and the reduced VDOS in Supplementary Fig. S5b, which are consistent with Fig. 1 in the main text. The estimated Boson peak frequency is around 1.3, quite close to the smaller system. We then show the transverse dynamical structure factors in a range of wavenumbers in Supplementary Fig. S5c, consistent with the results in Fig. 3a,b in the main text. The log-normal contribution from the quasi-localised modes is persistent around the Boson peak frequency. Furthermore,

similar to Fig. 3c, the longitudinal dynamical structure factors are dominated by the quasi-elastic components in the wavenumber and frequency range studied and are thus not shown here. To show the appearance of string- and ring-like motions (i.e. stringlets, see more discussion in Sec. VI) around the Boson peak frequency as observed in Fig. 6c in the main text, we use a simpler method for the larger system by calculating the particle-level vibrability [8]:

$$\Psi_i = \sum_{l=1}^{N_l} \frac{1}{\omega_l^2} |\vec{e}_{l,i}|^2 \tag{S7}$$

in which N_l is the number of vibrational modes around the Boson peak frequency. ω_l and $\vec{e}_{l,i}$ are the angular frequency and corresponding eigenvector of particle i for mode l. The Ψ_i field is shown in Supplementary Fig. S5d, in which the stringlets can be vividly seen. We also confirm its correlation to the fast β modes based on the Debye-Waller factor as in the main text. The consistency of the results between the small and large systems in all these aspects demonstrates the weak finite-size effect on our study.

III. Studies of additional two-dimensional models concerning the generality of our findings

To consider the generality of the quasi-localised modes in contributing to the Boson peak, we study two additional distinct two-dimensional glass models to account for the effects of long-ranging interactions and directional bondings.

As an example of systems with long-range attractions, we employ the two-dimensional version of the Kob-Andersen binary Lennard-Jones mixture of particles A and B of equal mass (2DKA) [9]. In brief, the particles interact via

$$U_{\alpha\beta}(r) = 4\epsilon_{\alpha\beta}\left[\left(\frac{\sigma_{\alpha\beta}}{r}\right)^{12} - \left(\frac{\sigma_{\alpha\beta}}{r}\right)^{6}\right], \tag{S8}$$

where $\alpha,\ \beta\ \in \{\mathrm{A},\ \mathrm{B}\}$, $\sigma_{\mathrm{AA}} = 1.0$, $\sigma_{\mathrm{BB}} = 0.88$, $\sigma_{\mathrm{AB}} = 0.8$, $\epsilon_{\mathrm{AA}} = 1.0$, $\epsilon_{\mathrm{BB}} = 0.5$, and $\epsilon_{\mathrm{AB}} = 1.5$. The potential is truncated and shifted at $r = 2.50\sigma_{\alpha\beta}$ up to the second derivatives. The simulated composition is 65 : 35 and number density is 1.20. The reduced units are used. This model has been proven to be stable against crystallisation in two dimensions and shows the glass-transition temperature around 0.33 [9]. We used $N = 8192$ particles under the NVT ensemble in our study. To generate the low-temperature glasses, we first equilibrate the system at a very high temperature $T = 5.0$ for a long time $t = 4000$. Next

we further equilibrate the liquid at $T = 2.1$ for another $t = 4000$, before quenching to $T = 0.1$ at a cooling rate of 10^{-3}. The glasses have been relaxed at the low temperature for $t = 2000$, and then energy minimisation via conjugate gradient algorithm is performed to obtain the inherent structure for further analyses. 50 independent simulations are carried out for ensemble average. This model includes longer-ranged attractive interactions, unlike the 2DPL model with purely short-range repulsions we employed. This makes the anharmonicity effect much weaker in the inherent state since, at low temperatures, the particles find themselves localised in deep wells where the minimum energies of the accessible well set the energy scale of the potential energy surface governing the materials dynamics [10]. The 2DPL model system is closer to the hard-sphere mixture and thus may exhibit entropic anharmonicity [11, 12]. Note that anharmonicity could give rise to localised modes and make a contribution to the Boson peak, as observed in some crystalline materials (see, e.g., Ref. 13 and 14) and in glass-forming liquids (see, e.g., Ref. 15). In addition, such Lennard-Jones interactions are commonly seen in many organic systems. We use the same analysis methods for this model as the main text. The estimated Boson peak frequency is about 1.3, close to the transverse Ioffe-Regel limit (~ 1.60). We show detailed characteristics of the transverse dynamical structure factors in Extended Data Fig. 8a,b. Phonon contribution dominates at low wavenumbers, whereas the log-normal contribution from quasi-localised modes around the Boson peak shows up and becomes prominent at high wavenumbers. On the contrary, such a signal is absent in the longitudinal dynamical structure factors (Extended Data Fig. 8c,d), consisting of quasi-elastic and phonon components in the wavenumber range studied. For this system, we also show $D(\omega)$, $D(\omega)/\omega$, the q-ω dependence of $S_{\mathrm{T}}(q,\omega)$, and the dispersion relations in Extended Data Fig. 9.

Additionally, as an example of systems with directional interactions, we study the two-dimensional spin liquid model (2DSL) proposed by our group [16–18]. The details of the potential can be found in the mentioned references. In brief, the potential for a pair $i-j$ is

$$U_{ij} = 4\epsilon \left[\left(\frac{\sigma}{r_{ij}}\right)^{12} - \left(\frac{\sigma}{r_{ij}}\right)^{6} - \Delta \left(\frac{\sigma}{r_{ij}}\right)^{6} f(\theta_i, \theta_j) \right], \tag{S9}$$

in which $f(\theta_i,\theta_j) = h(\frac{\theta_i-\theta_0}{\theta_c}) + h(\frac{\theta_j-\theta_0}{\theta_c}) - \frac{64}{35\pi}\theta_c$. $h(x) = 1 - 3x^2 + 3x^4 - x^6$ if $-1 < x < 1$ otherwise 0. θ_i is the angle between the positional vector $\vec{r}_{ji} = \vec{r}_j - \vec{r}_i$ and the unit vector $\vec{u}_i$ that represents the orientation of the axis of particle i. We use $\theta_0 = 126^\circ$ and

$\theta_c = 53.1°$. This model incorporates directional interactions, which energetically favours the formation of isolated pentagons (see Extended Data Fig. 10a). It simulates single-component systems with a wide range of fragility tuned by the parameter Δ. The higher Δ is, the stronger the liquid will be [17]. In this study, we choose a strong liquid with $\Delta = 0.80$ and a total of $N = 8192$ atoms. The NPT ensemble with a pressure $P = 0.50$ is used. The glass-transition temperature is thus about 0.166. To create the low-temperature glasses, we first equilibrate the system at $T = 0.71$ for $t = 3000$, and then quench to the low temperature $T = 0.01$ at a rate of 10^{-4}. We then relax the samples for $t = 2000$ before obtaining the inherent structures by the steepest descent algorithm. 50 independent simulations are carried out for ensemble average. The reduced units are used. For this model, the relationship between the Boson peak frequency ($\omega_{\rm BP} = 1.4$) and the transverse Ioffe-Regel limit has been well established [17]. The structural and dynamical properties during the glass transition have also been studied before [16–18]. We show the transverse dynamical structure factors at some exemplified wavenumbers in Extended Data Fig. 10b. The quasi-localised modes appear around $\omega_{\rm BP}$ at high wavenumbers (above the transverse Ioffe-Regel limit wavenumber), consistent with our findings in the main text and the 2DKA system described above.

These results indicate that our findings are universal for systems with long-range attractions, directional bondings, and a wide range of fragility. The extension to three-dimensional systems is intriguing for future study.

IV. Particle size ratio effect

In our 2DPL model, we use the fixed particle size ratio of 1.4, which has been shown to have the excellent glass-forming ability and form stable glasses [19]. We also check the size ratio of 1.2 and 1.6 for the 2DPL model. As shown in Supplementary Fig. S6, the system is easily phase-separated and even crystallised partially in these models. In addition, as shown above, we have found consistent results in the binary 2DKA model (size ratio: 1/0.88) and in the monodisperse 2DSL model. This also indicates that our conclusions are robust for different particle size ratios systems.

V. Analyses of atomic-scale features and their correlation with the vibrational modes

We identified isolated quasi-localised modes (QLMs) with four-leave patterns at a very low frequency and the stringlets related to the Boson peak in our model, as depicted in Fig. 6

in the main text. Now we are trying to check their possible correlation with the fluctuations of some atomic-scale features of the glassy state. The first candidate is the local volume, which is measured by standard Voronoi tessellation, as shown in Extended Data Fig. 7a. The second is the local chemical composition c_α (see Extended Data Fig. 7b), which is defined as the fraction of the atoms of type α in the first coordination shell of a centre of type α [20]. The third is the local potential energy in Extended Data Fig. 7c. In principle, these local quantities fluctuate independently, although the local Voronoi area shows a correlation with local composition in the present 2DPL model. We also measured the local shear moduli using the local fluctuation formula following Ref. [21]. There are two independent shear moduli in two dimensions: simple shear (G_s) and pure shear (G_p). The corresponding local moduli are shown in Extended Data Fig. 7d,e. However, compared to Fig. 6 in the main text, all these local properties are not correlated with QLMs and stringlets. Although there may be a characteristic wavenumber associated with the mechanical heterogeneity, it requires better statistics to estimate accurately. However, the visual inspection tells us that these quantities are not responsible for the Boson peak and QLMs.

We also stress that if the spatial heterogeneity of elasticity is the origin of phonon scattering, not only the transverse but also the longitudinal phonons should be scattered. However, there is no indication of the anomaly in the propagation of the longitudinal phonons around the characteristic wavenumber. This fact also indicates that the Boson peak originates from the resonant scattering by quasi-localised modes rather than the scattering due to spatial elastic heterogeneity.

Concerning the dynamic nature of QLMs, we analyse the non-affine displacement fields excited by quasi-static athermal deformation with a minimal strain, following Ref. [22]. As a reference, we first show the transverse component of the lowest non-zero frequency vibrational mode obtained by diagonalising the Hessian matrix in Extended Data Fig. 7g. The isolated QLMs showing four-leave patterns are visible, as also shown in Fig. 6a in the main text. The non-affine displacement field obtained by uniaxial tension is shown in Extended Data Fig. 7h, in which the major QLM is not excited. More importantly, the non-affine displacement field obtained by simple shear (see Extended Data Fig. 7i) shows a feature quite similar to the eigenvector field. This indicates that the excitation of QLMs depend externally on the deformation method and internally on their alignment in space. We only show some preliminary results on the mechanical analyses here for clarification.

More detailed results will be reported somewhere else in the future. We also estimate the spatial correlation of the non-affine displacement field in Extended Data Fig. 7f. A super large characteristic length scale ($\xi \sim 35$) is found from the zero-crossing point to the anti-correlation regime [22, 23]. Based on the measured dispersion relations, the corresponding frequencies ($\omega_{\mathrm{T,L}} = c_{\mathrm{T,L}}\frac{2\pi}{\xi}$) for the transverse and longitudinal vibrations are estimated as 0.86 and 2.34, respectively. The Boson peak frequency (~ 1.41) sits in-between, which is actually similar to the case in Ref. [23].

However, the relevant mode should be transverse since the deformation modes are transverse. Since the corresponding transverse phonon frequency (~ 0.86) is far below the Boson peak frequency (~ 1.41), we may say that there is no direct correspondence between them. Consistent with this, the non-affine displacement pattern is much coarser than the patterns of the Boson peak intensity field and the quasi-localised modes (see Fig. 6 in the main text), indicating that it has little correlation with them.

VI. Properties of stringlets that mainly contribute to the Boson peak

We note that the string-like structures are quite common in the disordered states, and there are actually different types of strings based on the observation timescales (see, for example, Ref. [24]). On the one hand, the strings in the fast dynamics regime are usually short and will grow upon heating. They are thus termed "stringlets" for clarity. This behavior has been observed in different systems [24–26]. On the other hand, the strings observed at the longer diffusion time is quite different in nature and will grow upon cooling, which relates to the increased activation free energy of molecular diffusion and structural relaxation time [24, 27, 28].

The string- and ring-like vibrations we observed belong to the former type. We find that the stringlets in our model system in the inherent states corresponding to low-temperature glassy solids are mostly curved (see Extended Data Fig. 5a), and closed rings are actually rare, i.e., most apparently ring-like structures are not completely closed. Therefore, we have characterised strings as linear objects and measured their sizes. We show the probability distribution of the string sizes in Extended Data Fig. 5b. Interestingly, it shows an exponential decay with increasing size, consistent with the results of a model anharmonic crystalline material [14], superheated Ni crystals [13], and a model metallic glass-forming material [29]. This result indicates the general nature of the string-like excitation in various materials.

VII. Supplementary Figures S1-S6 of the 2DPL model

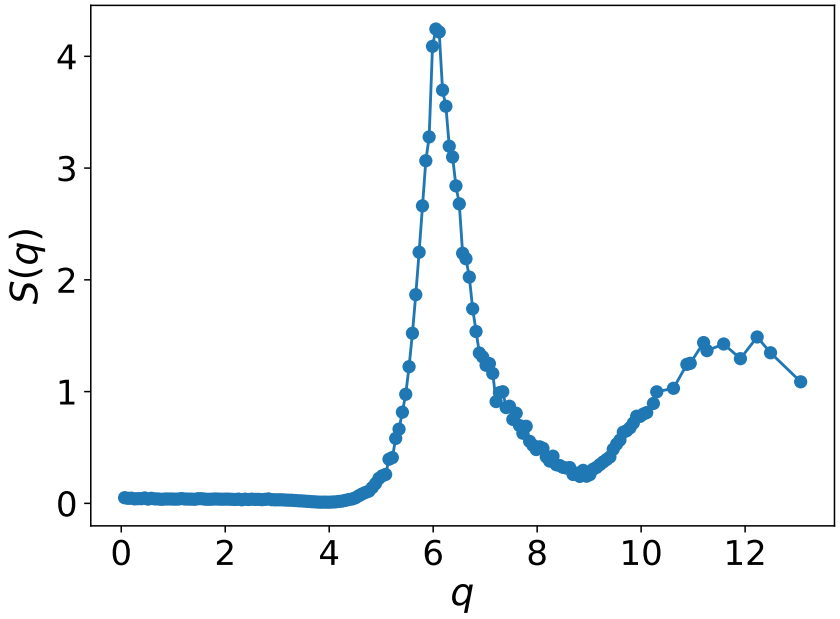

Supplementary Fig. S1. **The static structure factor.** This typical structure factor for an amorphous solid shows a first peak positioned at $q \approx 6.0$.

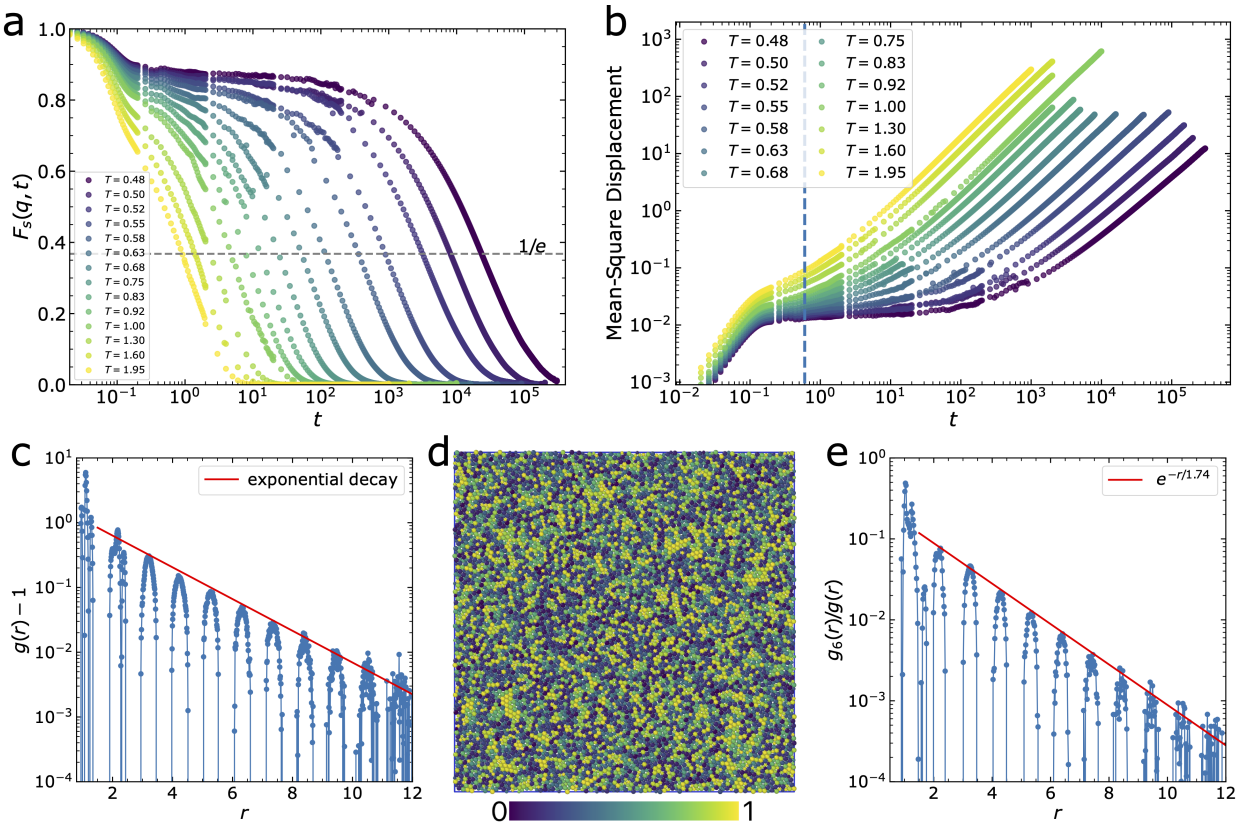

Supplementary Fig. S2. **The structural relaxation dynamics and structural characterisation. a,** The self-intermediate scattering functions at various temperatures. **b,** The mean-square displacements at various temperatures. The dashed line demonstrates a caging time. **c,** The pair correlation function of the glassy state, showing the exponential decay. **d,** Spatial distribution field of the local hexatic order. **e,** Spatial correlation of the local hexatic order, which rapidly decays exponentially (the correlation length is shorter than 2).

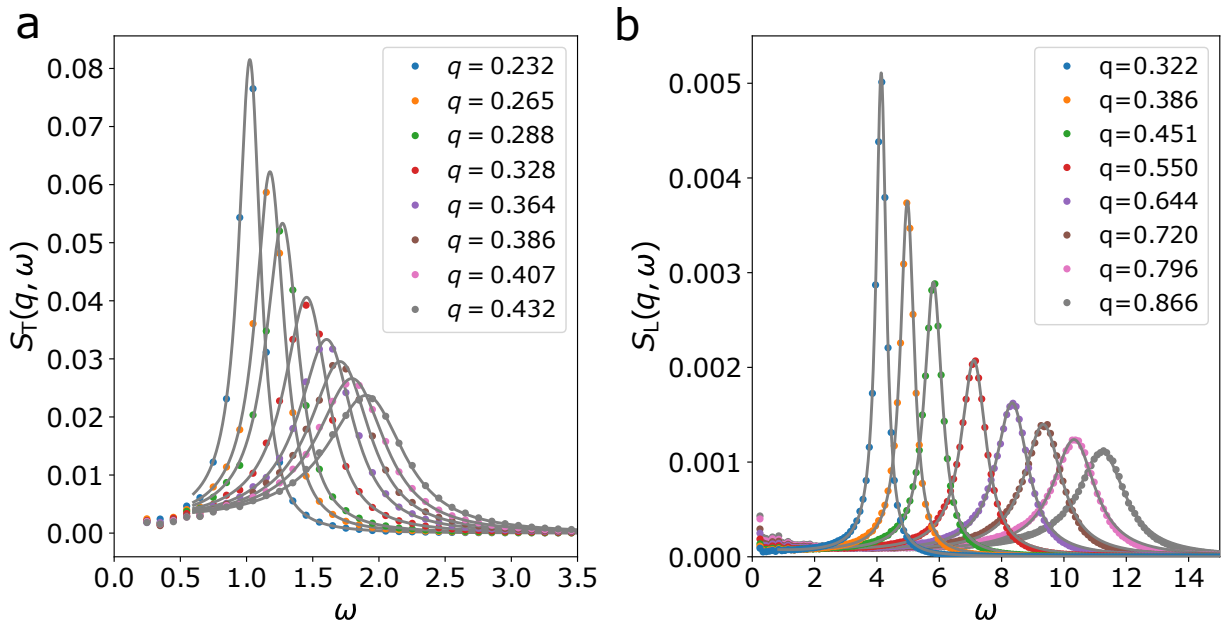

Supplementary Fig. S3. **The dynamical structure factors at low wavenumbers. a,** The transverse dynamical structure factors fitted by DHO (see equation (1) in the main text), which gives the characteristic frequency $\Omega_T(q)$ and damping coefficient $\Gamma_T(q)$. With increasing q, the phononic peak is broadened, indicating damping of phonons. **b,** The longitudinal dynamical structure factors fitted by equation (2) in the main text. Similar to the transverse component, the phononic frequency and broadness both increase with increasing q. At low q, the quasi-elastic component becomes very weak and invisible.

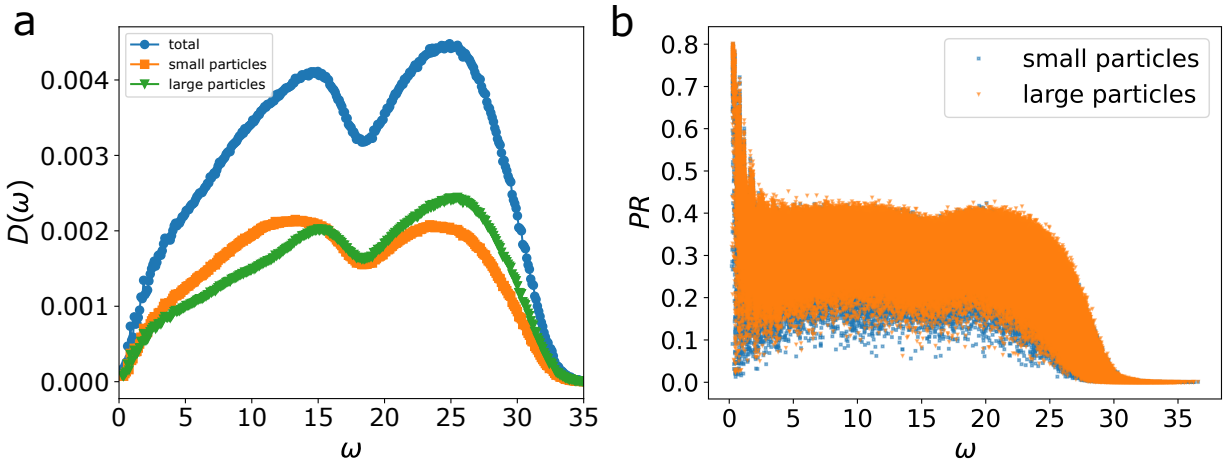

Supplementary Fig. S4. **Properties of the normal modes of atomic species. a,** The VDOS of the small and large particles compared to the overall VDOS. The difference of the VDOS between the two species is minimal, especially at low frequencies. The VDOS is estimated as $D(\omega) = \frac{1}{2N-2}\sum_{\lambda}(\sum_{\kappa}||\mathbf{e}_{\lambda}||^2)\delta(\omega-\omega_{\lambda})$, in which κ represents small or large particles. **b,** The participation ratios of the small and large particles over the whole frequency range. It is evident that the two species show nearly identical behaviours. These results demonstrate that small and large particles are both involved in the vibrational modes with little difference.

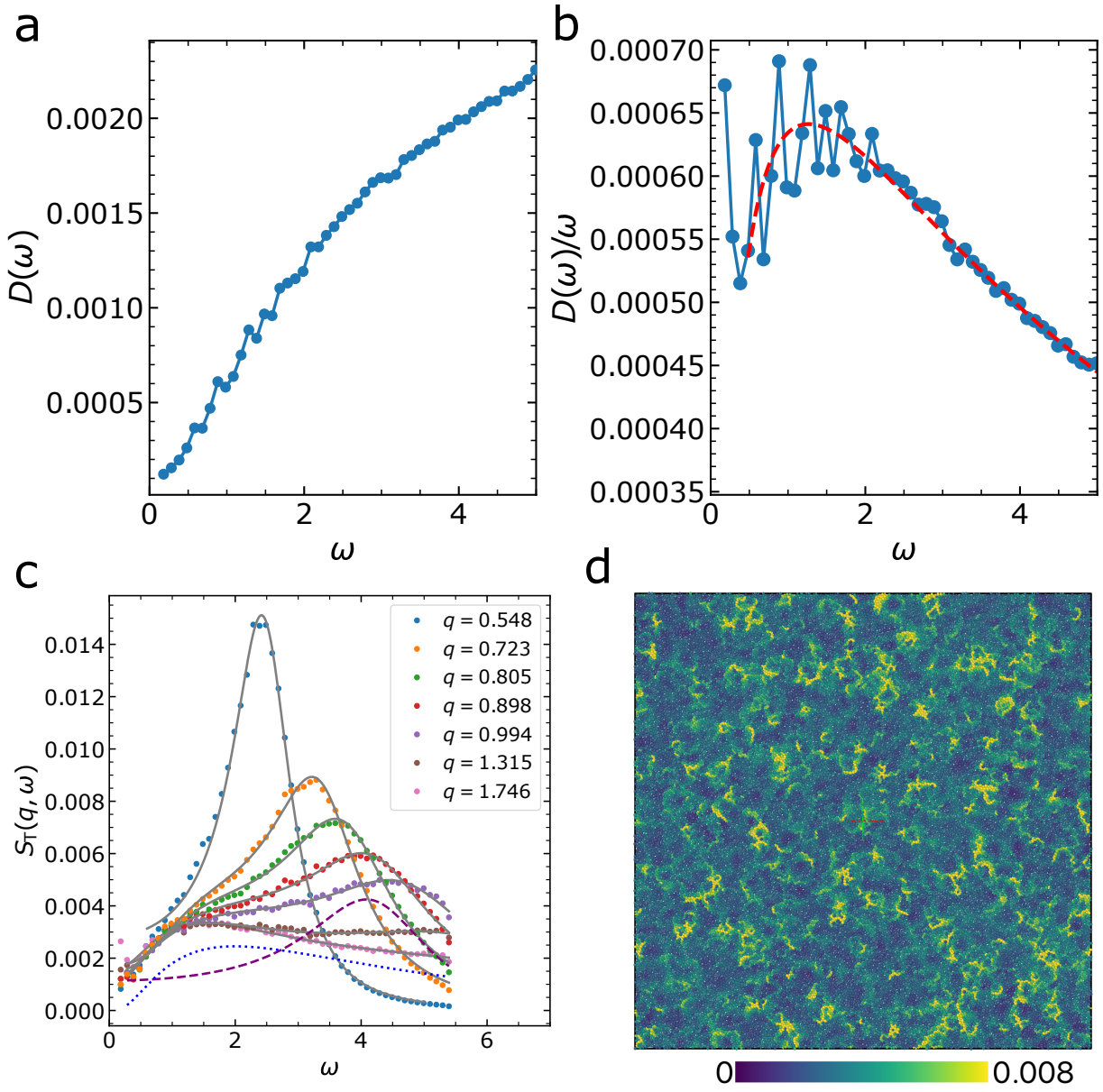

Supplementary Fig. S5. **Vibrational properties of the larger system with $N = 32768$ particles. a,** VDOS at low frequencies, which increases with ascending frequency. **b,** The reduced VDOS shows the Boson peak that can be described by a log-normal function (dashed red line). **c,** The transverse dynamical structure factors at several wavenumbers in the low-frequency range. Similar to Fig. 3a,b in the main text, the solid grey lines are fits to equation (1) in the main text. As an example, the dotted blue line and the dashed purple line represent the log-normal contribution and the phonon contribution at $q = 0.898$, respectively. **d,** Spatial distribution of atomic-level vibrability Ψ_i around the Boson peak frequency.

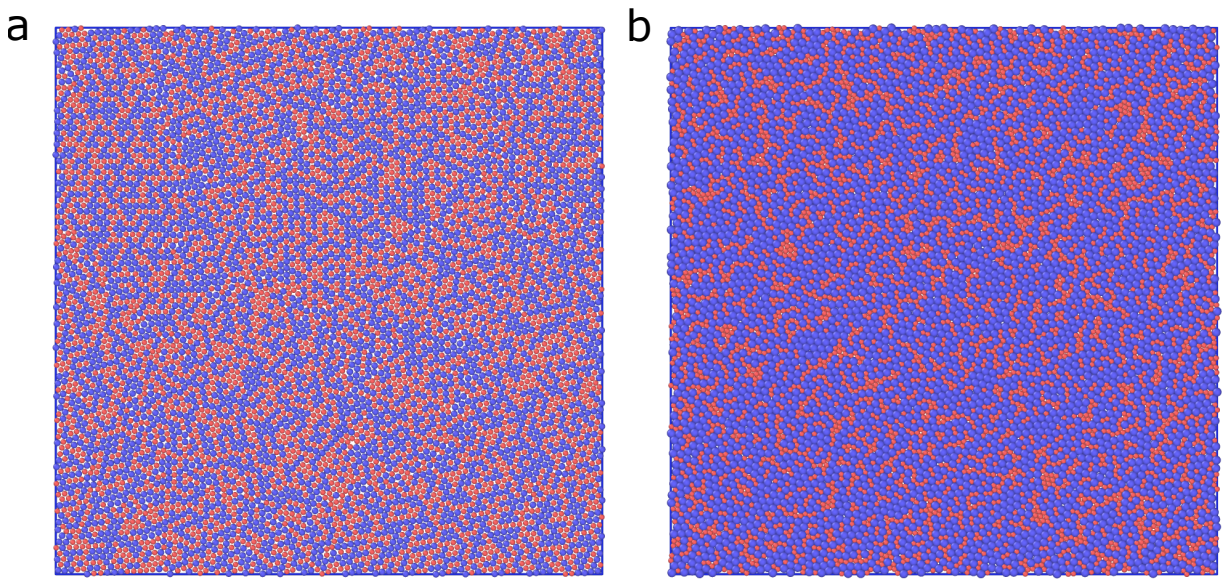

Supplementary Fig. S6. Configurations of low-temperature solids for binary mixtures with the size ratio of 1.2 (**a**) and 1.6 (**b**) interacting with the inverse-power law potential. Blue particles have a larger size.

VIII. Supplementary References

[1] Kapteijns, G., Bouchbinder, E. & Lerner, E. Universal nonphononic density of states in 2d, 3d, and 4d glasses. *Phys. Rev. Lett.* **121**, 055501 (2018).

[2] Lerner, E. & Bouchbinder, E. A characteristic energy scale in glasses. *J. Chem. Phys.* **148**, 214502 (2018).

[3] Douglas, J. F., Pazmino Betancourt, B. A., Tong, X. & Zhang, H. Localization model description of diffusion and structural relaxation in glass-forming CuZr alloys. *J. Stat. Mech.* 054048 (2016).

[4] Mahmud, G., Zhang, H. & Douglas, J. F. Localization model description of the interfacial dynamics of crystalline Cu and Cu64Zr36 metallic glass films. *J. Chem. Phys.* **153**, 124508 (2020).

[5] Mahmud, G., Zhang, H. & Douglas, J. F. Localization model description of the interfacial dynamics of crystalline Cu and Cu64Zr36 metallic glass nanoparticles. *Eur. Phys. J. E* **44**, 33 (2021).

[6] Zhang, H., Wang, X. & Douglas, J. F. Localization model description of diffusion and structural relaxation in superionic crystalline UO2. *J. Chem. Phys.* **151**, 071101 (2019).

[7] Tah, I., Sengupta, S., Sastry, S., Dasgupta, C. & Karmakar, S. Glass transition in supercooled liquids with medium-range crystalline order. *Phys. Rev. Lett.* **121**, 085703 (2018).

[8] Tong, H., Hu, H., Tan, P., Xu, N. & Tanaka, H. Revealing inherent structural characteristics of jammed particulate packings. *Phys. Rev. Lett.* **122**, 215502 (2019).

[9] Brning, R., St-Onge, D. A., Patterson, S. & Kob, W. Glass transitions in one-, two-, three-, and four-dimensional binary Lennard-Jones systems. *J. Phys. Condens. Matter* **21**, 035117 (2008).

[10] Simonazzi, R. & Tenenbaum, A. Anomalous fluctuations in low-temperature molecular dynamics simulations. *Phys. Rev. E* **54**, 964–967 (1996).

[11] Khrapak, S., Kryuchkov, N. P., Mistryukova, L. A. & Yurchenko, S. O. From soft- to hard-sphere fluids: Crossover evidenced by high-frequency elastic moduli. *Phys. Rev. E* **103**, 052117 (2021).

[12] Yurchenko, S. O., Komarov, K. A., Kryuchkov, N. P., Zaytsev, K. I. & Brazhkin, V. V. Bizarre behavior of heat capacity in crystals due to interplay between two types of anharmonicities.

J. Chem. Phys. **148**, 134508 (2018).

[13] Zhang, H., Khalkhali, M., Liu, Q. & Douglas, J. F. String-like cooperative motion in homogeneous melting. *J. Chem. Phys.* **138**, 12A538 (2013).

[14] Zhang, H., Wang, X., Chremos, A. & Douglas, J. F. Superionic UO2: A model anharmonic crystalline material. *J. Chem. Phys.* **150**, 174506 (2019).

[15] Douglas, J. F. & Xu, W.-S. Equation of state and entropy theory approach to thermodynamic scaling in polymeric glass-forming liquids. *Macromolecules* **54**, 3247–3269 (2021).

[16] Shintani, H. & Tanaka, H. Frustration on the way to crystallization in glass. *Nat. Phys.* **2**, 200–206 (2006).

[17] Shintani, H. & Tanaka, H. Universal link between the boson peak and transverse phonons in glass. *Nat. Mater.* **7**, 870–877 (2008).

[18] Tanaka, H., Kawasaki, T., Shintani, H. & Watanabe, K. Critical-like behaviour of glass-forming liquids. *Nat. Mater.* **9**, 324–331 (2010).

[19] Speedy, R. J. Glass transition in hard disc mixtures. *J. Chem. Phys.* **110**, 4559–4565 (1999).

[20] Hu, Y.-C. & Tanaka, H. Physical origin of glass formation from multicomponent systems. *Sci. Adv.* **6**, eabd2928 (2020).

[21] Mizuno, H., Mossa, S. & Barrat, J.-L. Measuring spatial distribution of the local elastic modulus in glasses. *Phys. Rev. E* **87**, 042306 (2013).

[22] Tanguy, A., Wittmer, J. P., Leonforte, F. & Barrat, J.-L. Continuum limit of amorphous elastic bodies: A finite-size study of low-frequency harmonic vibrations. *Phys. Rev. B* **66**, 174205 (2002).

[23] Leonforte, F., Boissire, R., Tanguy, A., Wittmer, J. P. & Barrat, J.-L. Continuum limit of amorphous elastic bodies. III. Three-dimensional systems. *Phys. Rev. B* **72**, 224206 (2005).

[24] Pazmio Betancourt, B. A., Starr, F. W. & Douglas, J. F. String-like collective motion in the α- and β-relaxation of a coarse-grained polymer melt. *J. Chem. Phys.* **148**, 104508 (2018).

[25] Zhang, H. & Douglas, J. F. Glassy interfacial dynamics of Ni nanoparticles: Part II Discrete breathers as an explanation of two-level energy fluctuations. *Soft Matter* **9**, 1266–1280 (2013).

[26] Zhang, H., Wang, X., Yu, H.-B. & Douglas, J. F. Fast dynamics in a model metallic glass-forming material. *J. Chem. Phys.* **154**, 084505 (2021).

[27] Donati, C. *et al.* Stringlike cooperative motion in a supercooled liquid. *Phys. Rev. Lett.* **80**, 2338–2341 (1998).

[28] Xu, W.-S., Douglas, J. F. & Sun, Z.-Y. Polymer glass formation: role of activation free energy, configurational entropy, and collective motion. *Macromolecules* **54**, 3001–3033 (2021).

[29] Zhang, H., Wang, X., Yu, H.-B. & Douglas, J. F. Dynamic heterogeneity, cooperative motion, and Johari-Goldstein β-relaxation in a metallic glass-forming material exhibiting a fragile-to-strong transition. *Eur. Phys. J. E* **44**, 56 (2021).